



Citation for published version:

Yang, C, Pei, X, Wu, Y, Yan, L, Yan, Y, Song, Y, Coyle, NM, Martinez-Urtaza, J, Quince, C, Hu, Q, Jiang, M, Feil, E, Yang, D, Song, Y, Zhou, D, Yang, R, Falush, D & Cui, Y 2019, 'Recent mixing of *Vibrio parahaemolyticus* populations', *ISME Journal*, vol. 13, no. 10, pp. 2578-2588. <https://doi.org/10.1038/s41396-019-0461-5>

DOI:

[10.1038/s41396-019-0461-5](https://doi.org/10.1038/s41396-019-0461-5)

Publication date:

2019

Document Version

Peer reviewed version

[Link to publication](#)

This is a post-peer-review, pre-copyedit version of an article published in The ISME Journal. The final authenticated version is available online at: <https://doi.org/10.1038/s41396-019-0461-5>

University of Bath

General rights

Copyright and moral rights for the publications made accessible in the public portal are retained by the authors and/or other copyright owners and it is a condition of accessing publications that users recognise and abide by the legal requirements associated with these rights.

Take down policy

If you believe that this document breaches copyright please contact us providing details, and we will remove access to the work immediately and investigate your claim.

Recent mixing of *Vibrio parahaemolyticus* populations

Chao Yang^{1#}, Xiaoyan Pei^{2#}, Yarong Wu¹, Lin Yan², Yanfeng Yan¹, Yuqin Song¹, Nicola Coyle³, Jaime Martinez-Urtaza⁴, Christopher Quince⁵, Qinghua Hu⁶, Min Jiang⁶, Edward Feil³, Dajin Yang², Yajun Song¹, Dongsheng Zhou¹, Ruifu Yang¹, Daniel Falush^{3*}, Yujun Cui^{1*}

1 State Key Laboratory of Pathogen and Biosecurity, Beijing Institute of Microbiology and Epidemiology, Beijing 100071, China;

2 National Center for Food Safety Risk Assessment, Beijing 100022, China

3 University of Bath, Bath, Somerset, United Kingdom

4 The Centre for Environment, Fisheries and Aquaculture Science, Dorset DT48UB, United Kingdom

5 Warwick Medical School, University of Warwick, Warwick, United Kingdom

6 Shenzhen Centre for Disease Control and Prevention, Shenzhen, 518055, China

[#]These authors contributed equally to the article

* Corresponding authors: D. F. (danielfalush@googlemail.com) or Y. C. (cuiyujun.new@gmail.com)

19 **Abstract**

20 Humans have profoundly affected the ocean environment but little is known about
21 anthropogenic effects on the distribution of microbes. *Vibrio parahaemolyticus* is found in
22 warm coastal waters and causes gastroenteritis in humans and economically significant
23 disease in shrimps. Based on data from 1,103 genomes, we show that *V. parahaemolyticus* is
24 divided into four diverse populations, VppUS1, VppUS2, VppX and VppAsia. The first two
25 are largely restricted to the US and Northern Europe, while the others are found worldwide,
26 with VppAsia making up the great majority of isolates in the seas around Asia. Patterns of
27 diversity within and between the populations are consistent with them having arisen by
28 progressive divergence via genetic drift during geographical isolation. However, we find that
29 there is substantial overlap in their current distribution. These observations can be reconciled
30 without requiring genetic barriers to exchange between populations if dispersal between
31 oceans has increased dramatically in the recent past. We found that VppAsia isolates from the
32 US have an average of 1.01% more shared ancestry with VppUS1 and VppUS2 isolates than
33 VppAsia isolates from Asia itself. Based on time calibrated trees of divergence within
34 epidemic lineages, we estimate that recombination affects about 0.017% of the genome per
35 year, implying that the genetic mixture has taken place within the last few decades. These
36 results suggest that human activity, such as shipping and aquatic products trade, are
37 responsible for the change of distribution pattern of this marine species.

38

39 **Introduction**

40 Hospitable environments for particular marine microbes can be separated by large distances
41 but whether dispersal barriers substantially influence their distribution and evolution is
42 unknown. There are many studies of distribution of marine microbes e.g.¹⁻⁴, but these
43 typically survey patterns of macro-scale diversity. Differences in species level or genus level
44 composition between locations are as likely to reflect environmental heterogeneity as
45 dispersal, making the patterns difficult to interpret. Recent spread of microbes between
46 continents has been documented for lineages that cause pathogenic infection of humans,
47 including notorious clonal groups within *V. parahaemolyticus* and *Vibrio cholerae*⁵⁻⁸.
48 However, these lineages are unusual in using humans as vectors, which might facilitate long-
49 range dispersal as in the case of the Haitian cholera outbreak⁹. We currently have little
50 information on rates of spread of the great majority of environmental organisms that do not
51 colonize large-animal hosts.

52

53 *V. parahaemolyticus* prefers warm coastal waters and causes gastroenteritis in humans^{10,11}.
54 Disease outbreaks became common from 1990s and became global, due to spread of
55 particular clones which are responsible for the great majority of recognized human
56 infections⁵, which has been attributed to factors such as El Niño and climate change¹²⁻¹⁴. It is
57 not clear to what extent this pattern is historically typical, or whether reflects better
58 surveillance and different patterns of usage of marine resources. These clones also make up a
59 small fraction of the *V. parahaemolyticus* diversity and only a very small fraction of strains
60 isolated during environmental sampling.

61

62 The *V. parahaemolyticus* genome undergoes high rates of homologous recombination with
63 other members of the species^{15,16}. We have previously found evidence that the species is split
64 into several populations¹⁶. Members of a population are not necessarily particularly related at
65 the clonal level, for example they may have recombined their entire genomes since sharing a
66 common cellular ancestor, but they are nevertheless on average more similar to each other
67 than to members of other populations because they have acquired DNA from a common gene
68 pool. Previously we found evidence of a single population with a well-mixed gene pool in
69 Asian waters and for one or more differentiated populations in the US¹⁶.

70

71 Here we use a larger and more broadly sampled collection of 1,103 genomes to examine the
72 global population structure of the species. We find four populations with different but
73 overlapping modern geographic distributions as well as a small number of hybrid strains.
74 Under the assumption that genetic exchange between strains is constrained by geography, the
75 current extent of overlap is too high to maintain the populations as distinct entities and we
76 conclude that most of this mixing is likely to have taken place within the last few decades,
77 possibly coinciding with the recent emergence of pandemic clones.

78

79 **Results and Discussion**

80 **Distribution of *V. parahaemolyticus* populations**

81 We analyzed genomes of 1,103 strains including 392 new strains sequenced as part of this
82 study. These strains were isolated from a mixture of sources during 1951-2016, and covered
83 24 countries (Supplementary Fig. 1 and Supplementary Table 1). Clonal relationships
84 between strains can be inferred from identifying long stretches of near-identity,
85 corresponding to regions of the genome that have been inherited by direct descent since the
86 strains shared a common ancestor, or, more simply, by the strains having a small number of

87 SNP differences between them genome wide, which can be revealed by the Neighbor-Joining
88 (NJ) tree (Fig. 1a). Based on criterion of high nucleotide identity, the dataset contains 13
89 clonal groups, with 10 associated with human disease and 3 associated with the environment
90 (Supplementary Table 1).

91

92 The presence of clonally related strains in the data complicates analysis of deeper population
93 structure, so we first removed closely related isolates to make a “non-redundancy” dataset of
94 469 strains, in which no sequence differed by less than 2,000 SNPs in the core genome
95 (Methods). We used fineSTRUCTURE to identify distinct populations¹⁷. In total, 115
96 populations were identified in this initial analysis, however most comprised only two or three
97 strains (Supplementary Fig. 2a). These are likely to be sets of strains that are clonally related,
98 so we removed all but one from each group and reran fineSTRUCTURE. After several
99 iterations of the same procedure, we identified four populations with between 10 and 217
100 members and two singletons (Supplementary Fig. 2b). These singletons might be hybrids or
101 representatives of otherwise unsampled populations.

102

103 The current distribution of the populations is shown in Fig. 2a. The great majority of isolates
104 from Asia (574/600) are assigned to VppAsia, with all but one of the remainder (VppUS1,
105 isolated from a shrimp farm in Thailand) being assigned to VppX. VppUS1 is found almost
106 entirely in the US and is most common in the Mexican Gulf, with 13 out of the 29 VppUS1
107 strains are isolated from there. VppUS2 is most common on the US Atlantic coast (20 of 42)
108 and has also been isolated several times in Northern Europe. VppX is most common on the
109 Pacific coast and the Northern part of the US coast. These patterns are not predominantly
110 determined by the spread of human disease clones, since similar patterns are observed if the
111 dataset is restricted to the 469 non-redundancy strains (Supplementary Fig. 3a). The
112 distribution of CG1, the pandemic clonal group that mostly belongs to sequence type (ST) 3⁵,
113 is similar to that of other VppAsia isolates (Supplementary Fig. 3b), while CG2 (ST36), an
114 epidemic group that is abundant in US and Canada⁸, has a similar distribution to that of
115 VppX isolates, except that it has not been isolated from Asia (Supplementary Fig. 3b). The
116 distribution of the four populations is also similar when analysis is restricted to strains from
117 the human disease (Supplementary Fig. 3c) or environment (Supplementary Fig. 3d).

118

119 The 1,103 genomes in this study have been collected for a variety of different purposes and
120 do not represent a defined environmental or epidemiological cohort. Furthermore, sampling

121 numbers in most locations are small and the coasts of Africa and Australia, for example are
122 almost entirely unsampled. Nevertheless, our results demonstrate that at a global scale,
123 geographic distributions of populations overlap considerably and that there is a substantial
124 difference in the frequencies of the populations in the waters of Asia and those of the US
125 Coast (Fig. 2a).

126

127 **Relationships amongst populations**

128 The populations have a modest level of differentiation at the nucleotide level (Supplementary
129 Table 2), with F_{st} values of around 0.1 approximately equivalent to that between humans
130 living on different continents¹⁸, implying that most common polymorphisms are shared
131 between populations. VppUS1 is the most diverse and isolates are no more similar to each
132 other in terms of mean SNP distance than they are to members of the other populations (Fig.
133 1b). However, according chromosome painting, which is based on haplotype similarity and
134 therefore more sensitive in detecting sharing of DNA due to common descent, all of the
135 members show substantially higher coancestry with other members of the population than
136 any of the other isolates in the dataset (Fig. 2b), implying that the population consists of
137 isolates that share ancestry, rather than being a collection of unassignable genomes. The other
138 populations have consistently lower distances with members of their own populations and
139 VppX and VppAsia are more closely related to each other than they are to VppUS1 and
140 VppUS2.

141

142 One explanation for the high diversity of VppUS1 is that it has frequently absorbed genetic
143 material from other populations. In order to test this hypothesis, while avoiding the effect of
144 clonal relationships within the population itself on estimates of relationships with other
145 populations, we painted the chromosomes of each of its members, using the members of the
146 other three populations as donors. A high diversity of painting palettes was observed from
147 VppUS1, with between 43% and 74% assigned to VppAsia and between 15% and 49% to
148 VppUS2 (Supplementary Fig. 4a). By contrast, the other three populations showed lower
149 levels of variation in assignment fractions in analogous paintings (Supplementary Fig. 4b-d).
150 Thus, VppUS1 owes its high diversity to being a hub for admixture, with input from both
151 VppUS2 and VppAsia. The members of VppUS1 in our sample are all clearly distinct in
152 ancestry profile from members of other populations (Fig. 2b), justifying the distinct
153 population label, but if gene flow levels were higher, it seems likely that the population

154 would lose its distinct identity and ancestry patterns would be better described by a
155 continuum than discrete population labels.

156

157 **Recent mixing of *V. parahaemolyticus* populations**

158 The observation of distinct populations is informative about patterns of migration in the past.
159 Population genetic theory implies that differentiation between demes can only arise and
160 persist if levels of migration between them are low, specifically on the order of magnitude of
161 one migrant per generation or less¹⁹. Once a migrant arrives in a deme, it progressively
162 imports DNA from other strains and becomes more and more similar to the other strains in its
163 new deme. The intuition behind the theory is that if too many strains are migrants, the demes
164 will progressively lose their distinct genetic profiles and merge into a single gene pool. This
165 theory has been developed for outbreeding eukaryotes²⁰ and bacterial populations deviate
166 from several of the assumptions of the theory, in ways that are currently not well understood,
167 making quantitative predictions impossible. Nevertheless, the qualitative expectation is that
168 most isolates should have the ancestry profile of the region, with only a small fraction of the
169 isolates having part ancestry from other locations.

170

171 The data differs from the qualitative predictions of migration-drift equilibrium because while
172 there are few strains of clearly intermediate ancestry in the dataset, many locations have
173 multiple strains from two or more of the four distinct populations that we have identified,
174 making it not obvious what deme they belong to. Asia is clearly the most likely ancestral
175 home range of *VppAsia* based on its high prevalence there but it is difficult to define
176 boundaries of likely ancestral ranges for the other three populations with any confidence
177 because the isolates assigned to those populations are too dispersed and they do not make up
178 a clear majority anywhere. Thus the current distribution is qualitatively inconsistent with
179 migration-drift equilibrium.

180

181 There are a number of factors which can in principle maintain subdivision when members of
182 particular populations are found in the same location. For example, it is possible that the
183 mechanism by which recombination occurs results in import occurring preferentially from
184 members of the same population. For example, barriers to recombination due to homology
185 dependent mismatch repair has been proposed to account for the differentiation between
186 phylogroups of *Escherichia coli*, despite high overall level of recombination²¹ because the
187 mechanism preferentially aborts recombination events between members of different

188 phylogroup. Other mechanisms that can generate barriers to gene flow are strain specific
189 phage, or differences in an ecological niche. However, the pattern of sharing of diversity is
190 very different in *V. parahaemolyticus* to that found in *E. coli*, with high nucleotide diversity
191 and low differentiation between them and there are few highly differentiated loci anywhere
192 within the core genome (Supplementary Fig. 5). It is difficult to conceive of a mechanistic
193 barrier encoded within the genomes or their phage that would effectively constrain
194 recombination between populations enough to explain the low number of hybrids within the
195 dataset as a whole, while also allowing the frequent recombination required to create the
196 freely mixed gene pools we see within populations. Therefore while it is difficult to rule out
197 this explanation, we do not consider it further.

198

199 We propose instead that barriers to movement of strains have reduced recently. Under this
200 hypothesis, it should be possible to approximately estimate the timescale on which mixing
201 has taken place, based on the amount of introgression found in locations where the different
202 populations now co-occur. Specifically, within our dataset, it is natural to compare the
203 VppAsia isolates within Asia and in North America. Since Asia has been least affected by
204 between continent migration (Fig. 2a), we predict that the VppAsia isolates in North America
205 should have more ancestry from other sources, that they have acquired recently in their new
206 locations. This prediction is borne out, a number of North America VppAsia isolates have
207 high levels of VppUS1 and VppUS2 ancestry and on average the North America VppAsia
208 isolates in the non-redundancy set of 469 strains have 1.01% more (in average 2.97% in
209 North America vs 1.96% in Asia) of their painting palette from VppUS sources than those
210 from Asia (Fig. 2b and Fig. 3a).

211

212 In order to provide a timescale for the acquisition of non-Asian ancestry, we examined the
213 evolution within the largest two clonal populations, CG1 and CG2. We removed
214 recombination regions, then ran BEAST²² to estimate a clock rate of 5.5×10^{-7} per site per
215 year, with very similar values for the two clonal complexes (Supplementary Fig. 6). There are
216 about 313 bases exchanged per mutation (Supplementary Fig. 7), so this implies a rate of
217 recombination of 1.7×10^{-4} per site per year. Thus if all of the import into the VppAsia
218 bacteria was from US populations, then it would imply it would take about 59 years (with
219 extreme lower and upper boundaries of 32-151 years, see methods) to acquire an extra 1.01%
220 ancestry at this rate of import.

221

222 We also examined the origin of imports within CG1, the global pandemic clonal group. As
223 for the VppAsia isolates, a higher fraction of the imports was from the two US populations
224 amongst the isolates found in the North America than for the isolates found in Asia itself.

225 This small difference in ancestry, corresponding to about 0.19% of the genome in total (Fig.
226 3c), has arisen during around 20 years since the beginning of global spread of CG1 in 1996.

227

228 These observations are consistent with a hypothesis that barriers to migration have become
229 substantially weaker within the last few decades, but do not constitute direct evidence that
230 patterns of gene flow between populations have changed. This hypothesis is empirically
231 testable although we do not have a suitable strain collection to facilitate it. For example, if the
232 Asian bacteria have arrived in large numbers in the US recently, then DNA from VppAsia
233 bacteria should make up a higher proportion of recent genetic imports than older ones.

234

235 In order to explain why the pattern of dispersal has changed recently, it is necessary to first
236 postulate reasons why dispersal was previously limited. We hypothesis that spread of bacteria
237 between oceans is limited by large distances between environments that are hospitable,
238 making it rare that bacteria survive transportation between them. Large mammals, seabirds
239 and other aquatic organisms travel large distances but do not necessarily provide habitats that
240 *V. parahaemolyticus* can colonize for the days or weeks required to get from one ocean to
241 another. Thus, we propose that dispersal between oceans did occur but was rare.

242

243 Humans have changed several aspects of the ocean environment, creating new habitats
244 through effluent discharge, warming and acidifying the oceans through climate change,
245 providing new mobile habitats on the hulls of ship and in ballast water and transporting
246 copepods and other marine organisms deliberately to facilitate aquaculture or more
247 accidentally through trade in marine products^{23,24}. Several of these could have facilitated
248 transmission of bacteria between oceans. Furthermore, *V. parahaemolyticus* can adapt to
249 colonize copepods²⁵ so that for example human-associated dispersal of species such as the
250 manila clam from Asia to the America and Europe²⁶ could be responsible for the high
251 frequency of Asian *V. parahaemolyticus* there. A single introduction via ballast water or
252 introduction of shellfish for aquaculture would typically have low values of propagule
253 pressure (a single event with few individuals), while recurring introductions through recently

254 increased human activity may contribute in a regular basis introducing trans-ocean migration
255 of *V. parahaemolyticus*.

256

257 Further work is required to narrow down the most important factors. To identify the
258 frequency of *V. parahaemolyticus* reads in extensive metagenomic sampling of the open
259 ocean would provide knowledge on natural transmission of this bacterium. One objection to a
260 direct human dispersal, rather than for example a role for climate change is that the absolute
261 number of bacteria transported by ships or trade is likely to be small. However, this objection
262 does not seem especially compelling. The absolute number of bacteria transported from one
263 ocean to another does not need to be very large; if bacteria are fit in their new environment,
264 they can multiply rapidly to constitute a substantial proportion of the bacteria in their new
265 habitat.

266

267 **Conclusions**

268 Our results support our earlier conclusion that *V. parahaemolyticus* is subdivided into distinct
269 geographical populations. We have identified 4 clearly differentiated populations, two of
270 which appear to have foci in the US (VppUS1 and VppUS2). A third is predominant in Asia,
271 while the ancestral home range of the fourth VppX is difficult to guess based on current
272 sampling. However, these ranges pose a puzzle, in that they overlap substantially, both for
273 environmental and human disease causing isolates, which show approximately similar
274 patterns of distribution. Hybrids are rare, for example, amongst VppAsia isolates found in the
275 US, most have ancestry profiles indistinguishable from strains found in Asia, while a handful
276 have less than 10% introgression from either of the two US populations. The simplest and
277 most parsimonious explanation is that previous barriers to migration have been reduced
278 recently, allowing bacteria to disperse rapidly between continents but that because bacterial
279 recombine relatively slowly (about 0.017% of their genome a year on average), there has not
280 had sufficient time to generate hybrids.

281

282 These results have two major implications. Firstly, they suggest that recent human activity
283 has disrupted long-standing barriers to genetic exchange in the oceans and that this has
284 affected microbial population structure. Secondly, changing global patterns of *V.*
285 *parahaemolyticus* disease incidence may be directly connected to changes in dispersal of the
286 species, rather than being specific to the small number of clonal lineages that are responsible
287 for most of the major outbreaks.

288

289 **Materials and Methods**

290 **Bacterial strains**

291 Totally 1,103 strains were used in this research, including 392 newly sequenced and 711
292 publicly available strains (Supplementary Table 1). The newly sequenced strains were
293 isolated in China during daily food surveillance in 2014. The remaining 711 publicly
294 available strains were downloaded from the NCBI database. The genomes of newly
295 sequenced strains are available in GenBank with the accession numbers listed in
296 Supplementary Table 1.

297

298 New sequenced strains were cultured in the LB-2% NaCl agar at 37 °C, and classical
299 phenol/chloroform method was used to the extract genomic DNA.

300

301 **Sequencing and assembly**

302 The whole genome DNA was sequenced by using Illumina Hiseq 4000. The pair-end
303 sequencing library with average insert size of 350 bp were build according to the
304 manufacture's introduction (Illumina Inc., USA). The read length is 150 bp and in average
305 500 Mb raw data were generated for each strain, which is corresponding to the sequencing
306 depth of approximately 100 fold. The adaptor sequence and low quality reads were filtered
307 and the clean reads were assembled by using SOAPdenovo v2.04²⁷ as described before¹⁶. The
308 number of contigs and average size of assemblies are 263 and 5.1 Mb, respectively.

309

310 **Variation Detection**

311 The SNPs were identified by aligning the *V. parahaemolyticus* genomes against with the
312 reference genome (RIMD 2210633) by using MUMmer²⁸ as previously described¹⁶, and only
313 bi-allelic SNPs were used in further analysis. As the number of detected SNPs would relate
314 with core-genome of different strain sets, we created multiple SNP sets by using different
315 strain sets when perform analysis in various purposes. Totally 462,214 SNPs were identified
316 from all 1,103 genomes, 650,683 SNPs were from 469 non-redundancy genomes, 355-8,921
317 SNPs were separately from 13 clonal groups.

318

319 **Population structure**

320 The NJ trees were built by using the TreeBest software
321 (<http://treesoft.sourceforge.net/treebest.shtml>) based on sequences of concatenated SNPs, and
322 were visualized by using online tool iTOL²⁹.

323

324 The population structure of *V. parahaemolyticus* was built based on the 469 non-redundancy
325 genomes set by using Chromosome painting and fineSTRUCTURE¹⁷ as described before¹⁶.

326 The fineSTRUCTURE result of all 469 non-redundancy genomes revealed that multiple
327 clonal signals still presented. Therefore we selected only one representative genome from
328 each clone, and combined them with the left genomes to perform another round of
329 Chromosome painting and fineSTRUCTURE analysis. After six iterations, we finally
330 obtained a set of 260 genomes with no clonal signals presented in the result (Supplementary
331 Fig. 2b). To balance the sampling size among different population, we selected 60 strains,
332 including 14-16 strains from each population and 2 hybrid strains, to repeat the
333 fineSTRUCTURE analysis (Supplementary Fig. 2c). The result further verify the population
334 structure of *V. parahaemolyticus* species. Population assignment based on fineSTRUCTURE
335 was consist with NJ tree (Fig. 1a) except for two strains, PCV08-7 and TUMSAT_H01_S4,
336 and one epidemic group, CG2. Strain PCV08-7 and TUMSAT_H01_S4 were assigned to
337 VppAsia and VppUS2 respectively by fineSTRUCTURE analysis, but in the NJ tree they are
338 more closely related with VppX strains. The CG2 strains were all assigned to VppX
339 populations by fineSTRUCTURE, but in NJ tree it was grouped with VppAsia strains.
340 The length of chunks were extracted from the output file of Chromosome painting based on
341 469 non-redundancy strains, to calculate the percentage of admixtures of different
342 populations for each non-redundancy genome (Fig. 2b).

343

344 **New designation of *V. parahaemolyticus* populations**

345 In previous study, we designated four *V. parahaemolyticus* populations, named Asia-pop, US-
346 pop 1, Hyb-pop 1, and Hyb-pop 2, separately, based on dataset of 157 genomes. Here with
347 more samples were used in distinguishing the population, we found a new population that
348 mostly isolated from US, and the previously defined Hyb-pop 1 were known as just several
349 hybrid strains, or representatives of otherwise unsampled populations. As evidences revealed
350 that *V. parahaemolyticus* populations are geographical clustered, we proposed novel
351 nomenclatures for them, which read as VppAsia, VppX, VppUS1 and VppUS2. The 'Vpp' is
352 abbreviation of '*V. parahaemolyticus* population'. The first three populations are

353 corresponding with previously defined Asia-pop, Hyb-pop 2 and US-pop 1, and the VppUS2
354 is the population newly identified in this study.

355

356 **Inference of substitution rate using BEAST**

357 Two clonal groups with large sample size, CG1 (n = 153, global pandemic group, also known
358 as O3:K6 and its sero-variants group) and CG2 (n = 92, an epidemic group that popular in
359 US, also known as serotype O4:K12), were selected to calculate molecular clock respectively
360 by using BEAST v1.8.3²². The variations that caused by recombination inferred by our
361 pipeline were excluded in substitution rates analysis. There are 10 of total 153 CG1 strains
362 revealed too many strain-specific SNPs and revealed unusual long branches in the NJ tree
363 even after removing the recombination variations (Supplementary Fig. 8), and similar pattern
364 was observed in 1 of total 92 CG2 strains. These 11 strains with unusual high number of
365 SNPs, and 22 strains with unknown isolation time, were excluded from BEAST analysis. We
366 implemented analysis under GTR + I and relaxed clock model with constant size coalescent.
367 The MCMC chain was run for 10^8 and sampling for every 5,000 generations. The effective
368 sample sizes of all inferred parameters were above than 200 in our results. The estimated
369 molecular clock based on CG1 genomes is 5.6×10^{-7} with 95% confidence interval (CI) of
370 $4.3\text{-}6.7 \times 10^{-7}$ per site per year, and 5.4×10^{-7} with 95% CI of $3.6\text{-}7.2 \times 10^{-7}$ for CG2
371 genomes. Here the average value, 5.5×10^{-7} , was used as the most likely estimate of *V.*
372 *parahaemolyticus* molecular clock. The extremes of 95% CI based on two clonal groups, i.e.,
373 $3.6\text{-}7.2 \times 10^{-7}$, were used as lower and upper 95% boundaries for ensuring that they
374 encompassed the true values as much as possible.

375

376 **Recombination detection and inference of recombination rate**

377 Totally 13 clonal groups with more than 10 strains (Supplementary Table 1), defined by intra-
378 group paired-distance less than 2,000 SNPs, were selected to be used in detection of
379 recombination events. We firstly used previously pipeline to detect recombination¹⁶. Briefly,
380 we recalled the SNPs for each clonal group because different datasets had different core-
381 genomes, and these SNPs were used to construct a NJ tree. Then PAML software package³⁰
382 was used to determine the SNPs of each branch. Assuming neutrality and no recombination,
383 the observed SNP density of a given region should follow the binomial distribution. We used
384 the sliding window method to identify regions that rejected the null hypothesis ($P < 0.05$) and
385 all SNPs in such windows were treated as recombined SNPs. We also used
386 ClonalFrameML³¹, a software based on maximum likelihood method, to detect bacterial

387 recombination within the same dataset. Sequence alignments of genomes for each clonal
388 group and the corresponding maximum-likelihood tree constructed using PHYML with HKY
389 model³², were used as input files and non-core regions were ignored during calculation. The
390 inferred recombination regions using ClonalFrameML are mostly consistent with our in-
391 house method (Supplementary Fig. 7).

392

393 Two sets of r/μ (ratio of size of recombination regions to the number of mutation sites) were
394 obtained through different methods. The value is 331 with 99% CI of 228-435 for our in-
395 house method and 295 with 99% CI of 186-404 for ClonalFrameML. The average value, 313,
396 was selected as r/μ of the *V. parahaemolyticus*. Concerning the molecular clock rate of $5.5 \times$
397 10^{-7} per site per year, the most likely recombination rate of *V. parahaemolyticus* is 1.7×10^{-4}
398 per site per year. We selected the extremes of r/μ from two sets of 99% CI, 186-435, to
399 calculate the lower and upper boundaries of recombination rate through multiplying the
400 extremes of the molecular clock, which obtained the results of $6.7 \times 10^{-5} - 3.1 \times 10^{-4}$ per site
401 per year. Accordingly, the time to obtained 1.01% of genome fragments would be 59 years
402 with extreme boundaries of 32-151 years.

403

404 **Identify the contribution of *V. parahaemolyticus* populations to pandemic genomes in** 405 **different geographical location**

406 We assigned CG1 strains into two groups according to their isolated location, with one
407 isolated from Asia and another isolated from North America. By using ClonalFrameML, we
408 inferred the recombination fragments that occurred on each strain. Totally 81 fragments were
409 found in Asia CG1 strains and 65 fragments were found in North America CG1 strains, with
410 total size of 221 kb and the median length of 1035 bp. Then we identify the possible donor
411 genome of these recombination fragments by align them against with 468 non-redundancy
412 genomes (excluding the CG1 genome from the dataset) using BLASTn, with a threshold of
413 coverage $\geq 80\%$ and identity $\geq 99.5\%$. The observed frequency of the donor genomes in
414 each population was calculated. For recombination fragments carried by Asia CG1 genomes,
415 the average value of their donor frequency in a population were taken as contribution
416 proportion of the corresponding population to the recipient sequences in Asia CG1 genomes,
417 and similarly, we obtained the contribution proportion of each population to the North
418 America CG1 genomes (Fig. 3c). We also try the relaxed identity thresholds (99.0%) in
419 BLASTn and acquired similar results.

420

421 **Acknowledgements**

422 We gratefully acknowledge Dr. Narjol Gonzalez-Escalona for contributing *V.*
423 *parahaemolyticus* genomes. This work is supported by the National Key Research &
424 Development Program of China (No. 2017YFC1601503, 2016YFC1200100 and
425 2017YFC1200800), Sanming Project of Medicine in Shenzhen (No. SZSM201811071) and
426 the National Natural Science Foundation of China (No. 31770001). J. Martinez-Urtaza were
427 funded by Natural Environment Research Council (NERC) project (No. NE/P004121/1).

429 **Author Contributions**

430 Y. C., D. F. and R. Y. designed the study and coordinated the project; X. P., L. Y., J. M., Q.
431 H., and D. Y. contributed strains for analysis; C. Y., X. P., Y. W, N. C., Y.Q. S., Y.J. S., Y. Y.,
432 M. J., C. Q., D. F. and Y. C. analyzed the data; E. F., J. M. and D. Z. provided insightful
433 comments, D. F. and Y. C. wrote the manuscript. All authors approved the final version of the
434 manuscript.

436 **Competing Financial Interests statement**

437 No

439 **References**

- 440 1. Brown, M.V., Ostrowski, M., Grzymiski, J.J. & Lauro, F.M. A trait based perspective on
441 the biogeography of common and abundant marine bacterioplankton clades. *Mar*
442 *Genomics* **15**, 17-28 (2014).
- 443 2. Yilmaz, P., Yarza, P., Rapp, J.Z. & Glockner, F.O. Expanding the World of Marine
444 Bacterial and Archaeal Clades. *Front Microbiol* **6**, 1524 (2015).
- 445 3. Kent, A.G., Dupont, C.L., Yooseph, S. & Martiny, A.C. Global biogeography of
446 Prochlorococcus genome diversity in the surface ocean. *ISME J* **10**, 1856-65 (2016).
- 447 4. Hellweger, F.L. *et al.* The Role of Ocean Currents in the Temperature Selection of
448 Plankton: Insights from an Individual-Based Model. *PLoS One* **11**, e0167010 (2016).
- 449 5. Nair, G.B. *et al.* Global dissemination of *Vibrio parahaemolyticus* serotype O3:K6 and
450 its serovariants. *Clin Microbiol Rev* **20**, 39-48 (2007).
- 451 6. Mutreja, A. *et al.* Evidence for several waves of global transmission in the seventh
452 cholera pandemic. *Nature* **477**, 462-5 (2011).
- 453 7. Weill, F.X. *et al.* Genomic history of the seventh pandemic of cholera in Africa.
454 *Science* **358**, 785-789 (2017).
- 455 8. Martinez-Urtaza, J. *et al.* Genomic Variation and Evolution of *Vibrio*
456 *parahaemolyticus* ST36 over the Course of a Transcontinental Epidemic Expansion.
457 *MBio* **8**(2017).
- 458 9. Chin, C.S. *et al.* The origin of the Haitian cholera outbreak strain. *N Engl J Med* **364**,
459 33-42 (2011).

- 460 10. Yeung, P.S. & Boor, K.J. Epidemiology, pathogenesis, and prevention of foodborne
461 *Vibrio parahaemolyticus* infections. *Foodborne Pathog Dis* **1**, 74-88 (2004).
- 462 11. Su, Y.C. & Liu, C. *Vibrio parahaemolyticus*: a concern of seafood safety. *Food*
463 *Microbiol* **24**, 549-58 (2007).
- 464 12. Ansele-Bermejo, J., Gavilan, R.G., Trinanés, J., Espejo, R.T. & Martínez-Urtaza, J.
465 Origins and colonization history of pandemic *Vibrio parahaemolyticus* in South
466 America. *Mol Ecol* **19**, 3924-37 (2010).
- 467 13. Martínez-Urtaza, J., Trinanés, J., González-Escalona, N. & Baker-Austin, C. Is El Niño a
468 long-distance corridor for waterborne disease? *Nat Microbiol* **1**, 16018 (2016).
- 469 14. Baker-Austin, C., Trinanés, J., González-Escalona, N. & Martínez-Urtaza, J. Non-
470 Cholera Vibrios: The Microbial Barometer of Climate Change. *Trends Microbiol* **25**,
471 76-84 (2017).
- 472 15. Yan, Y. *et al.* Extended MLST-based population genetics and phylogeny of *Vibrio*
473 *parahaemolyticus* with high levels of recombination. *Int J Food Microbiol* **145**, 106-12
474 (2011).
- 475 16. Cui, Y. *et al.* Epidemic Clones, Oceanic Gene Pools, and Eco-LD in the Free Living
476 Marine Pathogen *Vibrio parahaemolyticus*. *Mol Biol Evol* **32**, 1396-410 (2015).
- 477 17. Lawson, D.J., Hellenthal, G., Myers, S. & Falush, D. Inference of population structure
478 using dense haplotype data. *PLoS Genet* **8**, e1002453 (2012).
- 479 18. Rosenberg, N.A. *et al.* Genetic structure of human populations. *Science* **298**, 2381-5
480 (2002).
- 481 19. Wright, S. Evolution in Mendelian Populations. *Genetics* **16**, 97-159 (1931).
- 482 20. Whitlock, M.C. & McCauley, D.E. Indirect measures of gene flow and migration: F_{ST}
483 not equal to $1/(4Nm + 1)$. *Heredity (Edinb)* **82 (Pt 2)**, 117-25 (1999).
- 484 21. Didelot, X., Méric, G., Falush, D. & Darling, A.E. Impact of homologous and non-
485 homologous recombination in the genomic evolution of *Escherichia coli*. *BMC*
486 *Genomics* **13**, 256 (2012).
- 487 22. Drummond, A.J., Suchard, M.A., Xie, D. & Rambaut, A. Bayesian phylogenetics with
488 BEAUti and the BEAST 1.7. *Mol Biol Evol* **29**, 1969-73 (2012).
- 489 23. Ruiz, G.M. *et al.* Global spread of microorganisms by ships. *Nature* **408**, 49-50 (2000).
- 490 24. Martínez-Urtaza, J. *et al.* Spread of Pacific Northwest *Vibrio parahaemolyticus* strain.
491 *N Engl J Med* **369**, 1573-4 (2013).
- 492 25. Martínez-Urtaza, J. *et al.* Ecological determinants of the occurrence and dynamics of
493 *Vibrio parahaemolyticus* in offshore areas. *ISME J* **6**, 994-1006 (2012).
- 494 26. Chiesa, S. *et al.* A history of invasion: COI phylogeny of Manila clam *Ruditapes*
495 *philippinarum* in Europe. *Fisheries Research* **186**, 25-35 (2017).
- 496 27. Luo, R. *et al.* SOAPdenovo2: an empirically improved memory-efficient short-read de
497 novo assembler. *Gigascience* **1**, 18 (2012).
- 498 28. Delcher, A.L., Salzberg, S.L. & Phillippy, A.M. Using MUMmer to identify similar
499 regions in large sequence sets. *Curr Protoc Bioinformatics* **Chapter 10**, Unit 10 3
500 (2003).
- 501 29. Letunic, I. & Bork, P. Interactive tree of life (iTOL) v3: an online tool for the display
502 and annotation of phylogenetic and other trees. *Nucleic Acids Res* **44**, W242-5
503 (2016).
- 504 30. Yang, Z. PAML 4: phylogenetic analysis by maximum likelihood. *Mol Biol Evol* **24**,
505 1586-91 (2007).

- 506 31. Didelot, X. & Wilson, D.J. ClonalFrameML: efficient inference of recombination in
507 whole bacterial genomes. *PLoS Comput Biol* **11**, e1004041 (2015).
508 32. Guindon, S. & Gascuel, O. A simple, fast, and accurate algorithm to estimate large
509 phylogenies by maximum likelihood. *Syst Biol* **52**, 696-704 (2003).
510

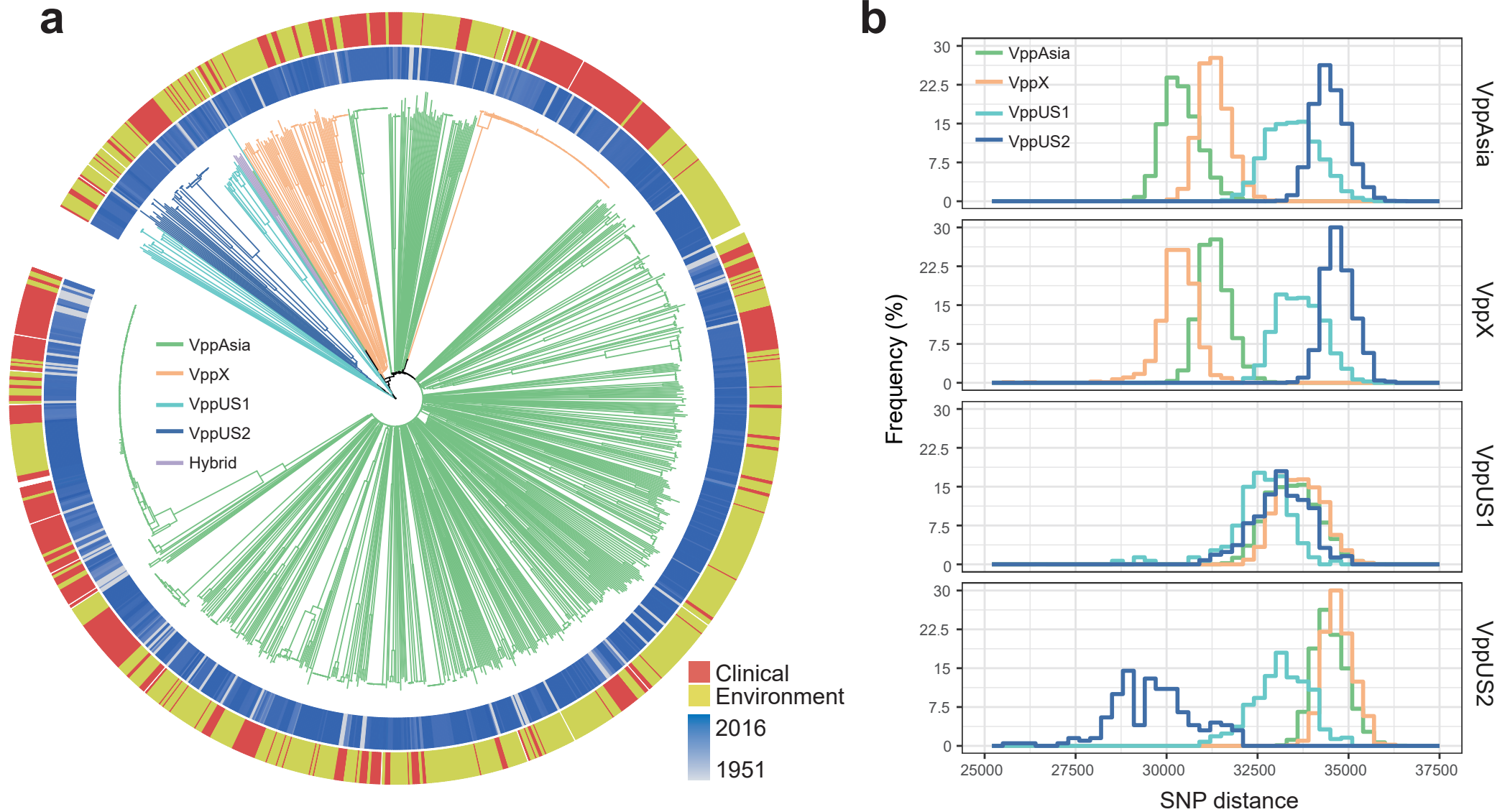


Figure 1. Population structure of *V. parahaemolyticus* and relationships within and between populations. (a) NJ tree of 1,103 *V. parahaemolyticus* strains based on 462,214 SNPs. Branch colors indicate populations defined by fineSTRUCTURE, green for VppAsia, orange for VppX, light blue for VppUS1, dark blue for VppUS2, purple for hybrid strains. The ring colors from inner to outer indicate isolation time and sample type, respectively. The blank indicates information not available. (b) SNP distance within and between populations based on 469 non-redundancy strains. Colors indicate populations and are consistent with branch colors of panel a.

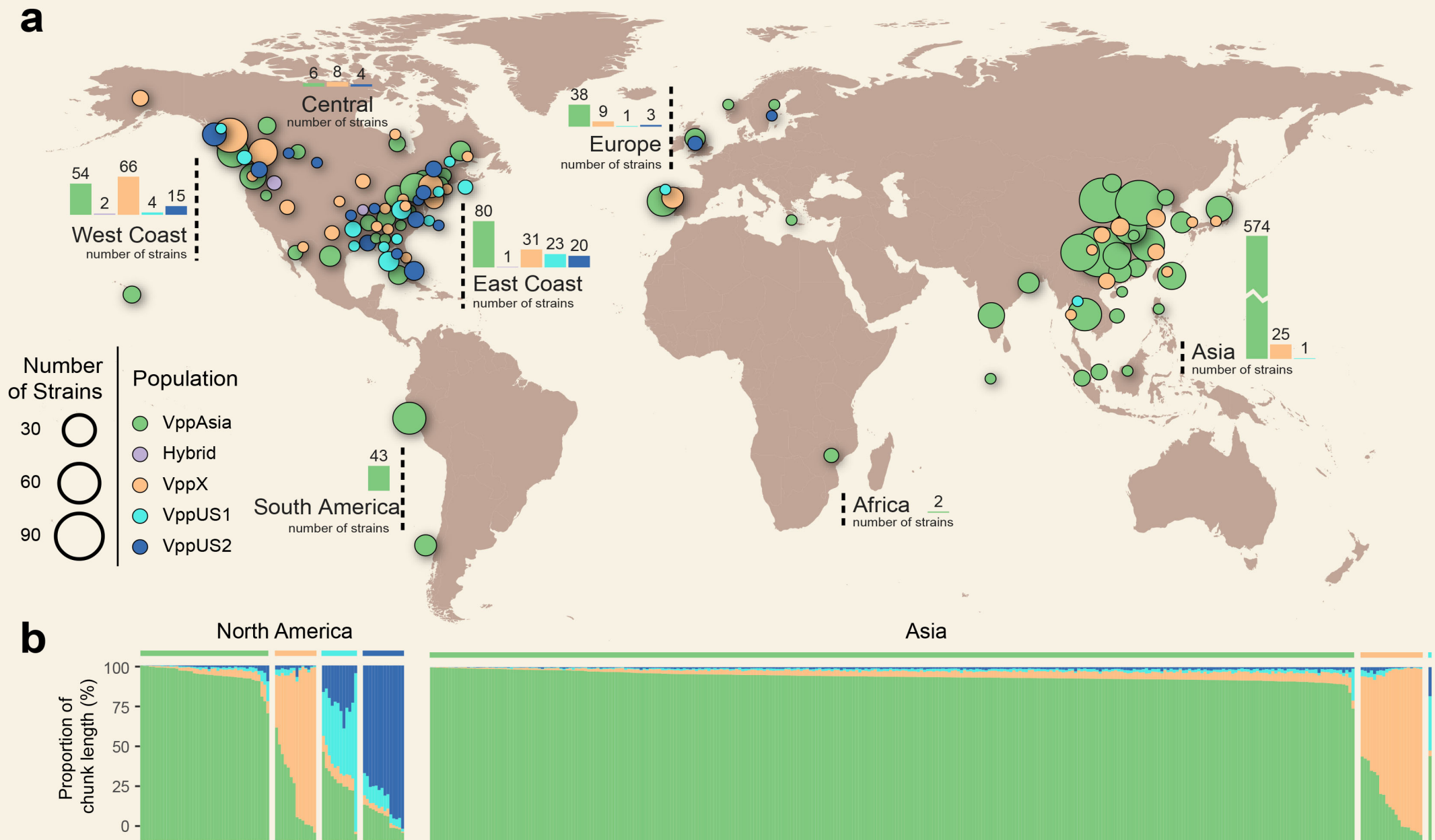


Figure 2. Geographical distribution and admixture of *V. parahaemolyticus* populations. Colors in circle and bar plot indicate populations and are as in Figure 1. Each circle indicates the population composition of a city/country, with radius in proportion to the sample size. Bar plot indicates the ancestry composition inferred by chromosome painting of two geographical regions: Asia and North America. Each vertical bar represents one non-redundancy strain and the proportion of color indicates the contribution of each population. Different populations are separated by blank vertical bar. Only strains with information of isolation location are included in panel a ($n = 1,008$) and panel b ($n = 422$).

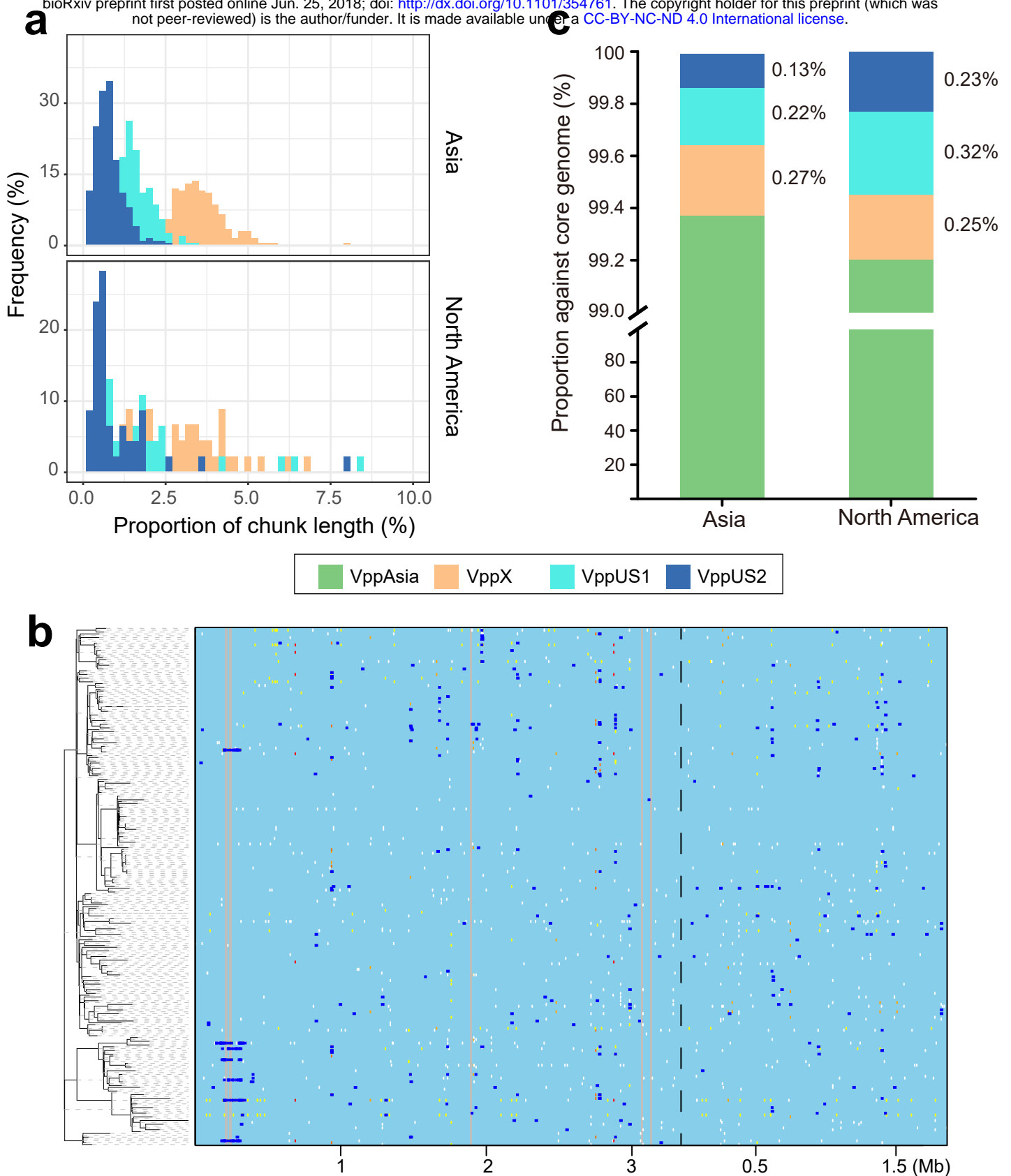


Figure 3. Recent mixing of *V. parahaemolyticus* populations. (a) Ancestry composition of three other *V. parahaemolyticus* populations in VppAsia strains in different geographical regions. The contribution from other populations to the VppAsia is inferred by chromosome painting. X axis indicates the proportion of contributed chunk length of a population in one strain and Y axis indicates the corresponding frequency. (b) ClonalFrameML recombination analysis of 141 CG1 strains. Left: ClonalFrameML reconstructed phylogeny. Right: dark blue horizontal bars indicate recombination events, grey areas indicate non-core regions. Two chromosomes are separated by dot line. (c) Source of recombination fragments of CG1 strains in different geographical regions. Y axis indicates the proportion of recombination fragments input from different population against core genome. Colors in (a) and (c) indicate four populations and are as in Figure 1.